

# Dynamics of fabric and dryer sheet motion in domestic clothes dryers

Jones, C. R.; Corona, A.; Amador, C.; Fryer, P. J.

DOI:

[10.1080/07373937.2021.1918706](https://doi.org/10.1080/07373937.2021.1918706)

License:

Creative Commons: Attribution (CC BY)

*Document Version*

Publisher's PDF, also known as Version of record

*Citation for published version (Harvard):*

Jones, CR, Corona, A, Amador, C & Fryer, PJ 2021, 'Dynamics of fabric and dryer sheet motion in domestic clothes dryers', *Drying Technology*, pp. 1-18. <https://doi.org/10.1080/07373937.2021.1918706>

[Link to publication on Research at Birmingham portal](#)

## General rights

Unless a licence is specified above, all rights (including copyright and moral rights) in this document are retained by the authors and/or the copyright holders. The express permission of the copyright holder must be obtained for any use of this material other than for purposes permitted by law.

- Users may freely distribute the URL that is used to identify this publication.
- Users may download and/or print one copy of the publication from the University of Birmingham research portal for the purpose of private study or non-commercial research.
- User may use extracts from the document in line with the concept of 'fair dealing' under the Copyright, Designs and Patents Act 1988 (?)
- Users may not further distribute the material nor use it for the purposes of commercial gain.

Where a licence is displayed above, please note the terms and conditions of the licence govern your use of this document.

When citing, please reference the published version.

## Take down policy

While the University of Birmingham exercises care and attention in making items available there are rare occasions when an item has been uploaded in error or has been deemed to be commercially or otherwise sensitive.

If you believe that this is the case for this document, please contact [UBIRA@lists.bham.ac.uk](mailto:UBIRA@lists.bham.ac.uk) providing details and we will remove access to the work immediately and investigate.



## Dynamics of fabric and dryer sheet motion in domestic clothes dryers

C. R. Jones, A. Corona, C. Amador & P. J. Fryer

To cite this article: C. R. Jones, A. Corona, C. Amador & P. J. Fryer (2021): Dynamics of fabric and dryer sheet motion in domestic clothes dryers, *Drying Technology*, DOI: [10.1080/07373937.2021.1918706](https://doi.org/10.1080/07373937.2021.1918706)

To link to this article: <https://doi.org/10.1080/07373937.2021.1918706>



© 2021 The Author(s). Published with license by Taylor and Francis Group, LLC



Published online: 12 May 2021.



Submit your article to this journal [↗](#)



Article views: 138





View related articles [↗](#)



View Crossmark data [↗](#)

# Dynamics of fabric and dryer sheet motion in domestic clothes dryers

C. R. Jones<sup>a</sup> , A. Corona<sup>b</sup>, C. Amador<sup>c</sup>, and P. J. Fryer<sup>a</sup> 

<sup>a</sup>School of Chemical Engineering, University of Birmingham, Edgbaston, Birmingham, UK; <sup>b</sup>P&G Fabric & Home Care Innovation Centre, Cincinnati, OH, USA; <sup>c</sup>P&G Technical Centres Limited, Longbenton, UK

## ABSTRACT

Positron emission particle tracking (PEPT) has been used to investigate the motion of radioactively labeled tracer particles attached to fabrics and solid fabric enhancer (SFE) delivery articles, such as dryer sheets, in the domestic clothes dryer. This work examines the dynamics of motion within the dryer across a range of operating conditions. Six regions within the dryer drum are identified, demonstrating the range of movements experienced by items during tumbling. These show clear correlation with existing flow regimes describing behavior of granular media in rotating drums. Fabric motion is primarily cataracting to maximize the surface area of fabric available to interact with drying air in the falling region, with some conditions moving toward centrifuging or cascading flows. Movement in the axial direction was significantly slower than the primary radial flow. Dryer sheets were more prone to centrifuging than fabrics, with significant time spent in contact with the drum wall. Conversely, a wool dryer ball was more likely to cascade, spending time mixed into the top of a fabric bed which forms in the impact and lifting regions. Behavior in this bed is primarily determined by frictional interactions with the drum wall, which subsequently affects behavior in the 5 remaining regions. The most significant changes to this behavior were observed when changing fabric moisture content and volumetric fill ratio, with wet fabrics and smaller load sizes both exhibiting faster falling speeds and spending more time in the fabric bed. The changes were most significant in the lifting, falling and detachment regions, with varying acceleration and shearing likely to influence both fabric wear and SFE delivery.

## ARTICLE HISTORY

Received 17 January 2021  
Revised 14 April 2021  
Accepted 14 April 2021

## KEYWORDS

Positron emission particle tracking (PEPT); tumble dryer; fabric motion; dryer sheet; dryer ball

## 1. Introduction

Clothes drying is a common household process based on a simple principle; fabrics tumble in a drum through a flow of hot air, aiding the evaporation of water remaining after washing. Existing literature has routinely considered the dryer using black box thermodynamic models.<sup>[1-3]</sup> This has led to recent improvements in dryer efficiency and the development of so called ‘high-efficiency’ appliances.<sup>[4,5]</sup> However, consumer perception of drying performance considers more than just final fabric moisture content.

Surface feel, odor, wrinkling, and static cling are important factors, difficult to control with changes to the drying process alone. These benefits may be delivered by the addition of solid fabric enhancers (SFE) to the dryer using products such as dryer sheets. During drying, the SFE mixture is transferred to items of clothing in surface-surface interactions. These include direct contact between dryer sheets and fabrics, indirect transfer via the drum wall and secondary transfer between fabrics, as

shown in [Figure 1](#). Without a full understanding of drying, development of these products has been limited to time and labor-intensive trial and error approaches. The behavior of items within the dryer, including interactions between fabrics, SFE coated articles and the dryer drum, will be significant in both the drying process and delivery of fabric care benefits. This work examines the dynamics of fabric and dryer sheet motion within the dryer to aid the development of new appliances, fabric enhancers, and delivery articles. The objective is to further understanding of behavior of these items throughout different regions of the dryer and along the length of the drying cycle (i.e., as moisture content decreases) for a range of consumer representative load conditions.

### 1.1. Motion in industrial rotating drums

Front loading domestic tumble dryers are fundamentally rotating drums, a unit operation which has been examined extensively. They are widely used in the

**CONTACT** C. R. Jones  crj341@student.bham.ac.uk  School of Chemical Engineering, University of Birmingham, Edgbaston, Birmingham B15 2TT, UK.

© 2021 The Author(s). Published with license by Taylor and Francis Group, LLC

This is an Open Access article distributed under the terms of the Creative Commons Attribution License (<http://creativecommons.org/licenses/by/4.0/>), which permits unrestricted use, distribution, and reproduction in any medium, provided the original work is properly cited.

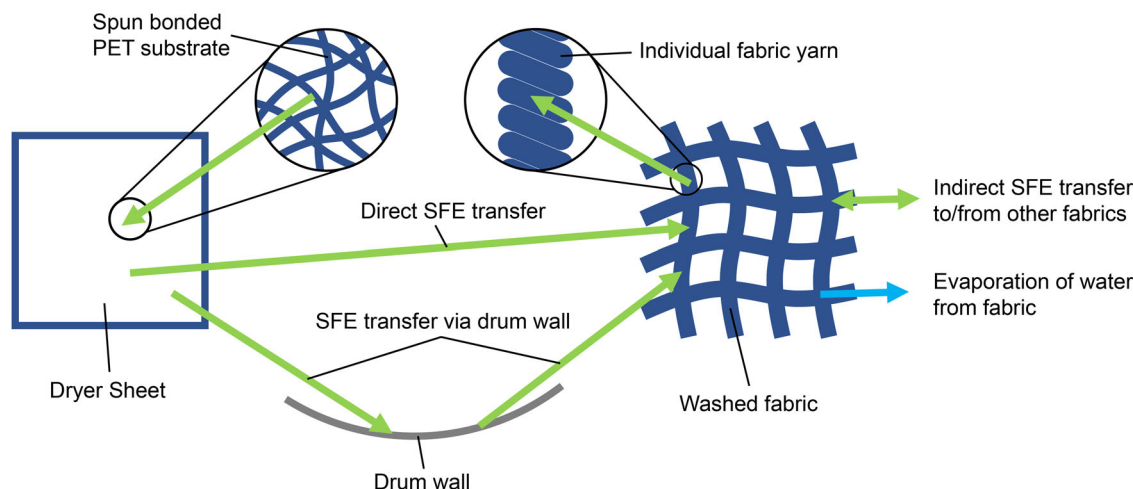


Figure 1. Schematic representation of the interactions involved in SFE delivery in the dryer drum.

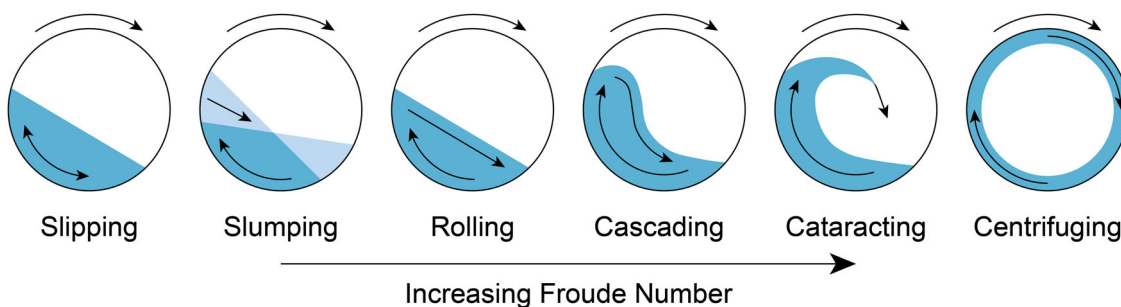


Figure 2. Flow regimes in rotating drums with increasing Froude number.<sup>[7]</sup>

chemical and pharmaceutical industries for the mixing, drying, and comminution of primarily particulate materials.<sup>[6]</sup>

Henein et al.<sup>[7]</sup> characterized flows in rotating drums in terms of the Froude number,  $Fr = \frac{\omega^2 R}{g}$ , where  $\omega$  is angular drum speed ( $\text{rad s}^{-1}$ ),  $R$  is drum radius (m) and  $g$  is gravitational acceleration ( $\text{m s}^{-2}$ ). This is the ratio of centripetal to gravitational forces. As Froude number increases for a given fill media, flow transitions through the regimes shown in Figure 2. Flows with higher Froude numbers (large diameter or fast-rotating drums) exhibit a cascading or cataracting motion due to the higher centripetal forces. For  $Fr > 1$ , the flow transitions to a centrifuging motion as centripetal forces outweigh gravitational forces. As flow transitions through these regimes the media is transported higher in the static bed before detaching. Cascading sets in when the surface layer begins to arch, forming a crescent shape. As  $Fr$  increases further, media is flung from the bed into the free space of the drum, falling over the static bed and reattaching toward the base in a cascading motion. In these regimes the assumption of static flow in the bed breaks, with sheared layers forming. With further increases of  $Fr$ , the media is flung a greater

distance across the drum until those at the extremes adhere to the wall giving full rotation in a centrifuging motion.<sup>[8,9]</sup> For the same drum design and rotational speed (i.e., constant  $Fr$ ), behavior is affected by the volumetric fill level of the drum and friction coefficient between the drum wall and media. Lower volumetric fill levels lead to more cataracting, or at the extreme centrifuging, motion. Increasing the friction coefficient between the drum wall and media or adding internal lifters to the drum has the same effect.<sup>[7]</sup>

In a rotating drum dryer, most evaporation occurs during the free fall period where the large surface contact between solid and gas phases, maximizes heat transfer from the hot air stream to the wet media.<sup>[10]</sup> To increase solid-gas interaction the Froude number must be chosen to ensure operation in the cataracting regime, where materials occupy the maximum drum volume.<sup>[7,11]</sup> Moving into the centrifuging or cascading regimes reduces interaction as material spends more time pressed against the outer drum wall or in the surface layer, respectively.

The Froude number shows drum size plays an important role. Other variables that influence motion include the volumetric fill ratio of media in the drum

and ratio of characteristic length of media to drum radius.<sup>[12]</sup> A number of scaling relationships have been reported based on the change of velocity with depth in the central flowing layer. These do not fit cascading or cataracting flows, such as those seen in the clothes dryer, due to the complex curved profile of the surface layer and shearing in the lifted bed. Govender<sup>[9]</sup> reviews relevant scaling laws for lower Froude numbers.

Most investigations of motion in rotating drums focus on a two-dimensional projection of the radial movement of media for the full axial depth of the drum. While some axial motion does occur, this is generally much slower than radial movement.<sup>[12]</sup> In systems where significant axial motion is required this must be induced through drum design using an axial incline or internal lifters.<sup>[13]</sup>

### 1.2. Visual analysis of fabric motion

Studying motion in rotating drums presents challenges due to the opaque nature of both the drum and fill media. Visual imaging techniques have been used to examine motion of textiles in domestic front-loading washing machines and tumble dryers. Yun et al.<sup>[14]</sup> developed a tracking method using a modified transparent washer and high-speed camera. Only a single fabric item was included, over a short time period, so data are unlikely to be fully representative of fabric motion.

The method was revised by Wei et al.<sup>[15]</sup> to investigate motion in a tumble dryer. Results for fabric motion are purely qualitative; however, some initial insight into bulk fabric movement in the dryer is given. Outline patterns were categorized according to four regimes, similar to those shown in Figure 2. The drying rate was highest in the cataracting regime, as expected.

Yu and Ding<sup>[16]</sup> and Yu et al.<sup>[17]</sup> used a similar high-speed visual tracking system with a thresholding method to identify the tracer fabric. A bulk region with little relative motion between fabrics was observed along the drum wall as items were lifted. These then detached and fell through a high velocity disperse region before impacting the drum wall and rapidly decelerating. This behavior is in line with a cataracting flow of granular media as discussed above.

Visual methods give useful insight into general fabric motion in the dryer, but have drawbacks. As the fabric is opaque, tracer fabrics can only be detected when adjacent to transparent walls. Location tracking based on the visible fabric area is also susceptible to

high error, and will be sensitive to load size and fabric size changes that impact visibility of the tracer, leading to inconsistencies in results.

### 1.3. Positron emission particle tracking

A number of nonvisual techniques have been employed to track motion in opaque drums, including MRI and X-Ray imaging.<sup>[9]</sup> One of the most successful methods is Positron Emission Particle Tracking (PEPT), developed at the University of Birmingham using a modified ADAC Forté medical PET scanner to allow detection of a radioactively labeled tracer.<sup>[18]</sup> Glass bead tracer particles can be produced by direct activation to produce a structural layer of the radionuclide Fluorine-18. This undergoes  $\beta^+$  decay, emitting a positron which annihilates with a nearby electron to produce two co-linear  $\gamma$ -ray photons. When a pair of coincident photons impact the detectors on either side of the system being investigated, their locations are recorded as a timestamped line of response, LoR. A tracking algorithm is then used to triangulate the location of the tracer particle.<sup>[19,20]</sup> Windows-Yule et al.<sup>[21]</sup> give a comprehensive review of the technique.

PEPT enables 3D tracking of particles traveling at high speed in opaque systems. This allows investigation of time averaged behavior for the full system, giving it many advantages over visual tracking. PEPT has been used extensively to study motion in rotating drums, including a study into fabric movement in a front-loading washing machine by Mac Namara et al.<sup>[22]</sup>

Recent advances in PEPT<sup>[23]</sup> have included development of a machine-learning based algorithm for tracer trajectory tracking. This calculates tracer coordinates based on the same LoRs as the older 'Birmingham' method, but with significantly improved accuracy and temporal resolution, able to locate a tracer particle every 0.25 ms with an error of less than 0.5 mm. The PEPT-ML algorithm uses a 2-pass clustering method based on the HDB-SCAN clustering algorithm,<sup>[24]</sup> outputting a set of highly accurate tracer trajectories for analysis. The algorithm used here was implemented in Python (v3.7.4) and is available from <https://github.com/uob-positron-imaging-centre/pept>.

## 2. Materials and methods

Drying experiments were carried out in PEPT using a Maytag 3LMEDC315FW 10.5 kg American style vented tumble dryer and Hotpoint V4D01P 4 kg



**Table 1.** Dryer specifications

Parameter	Hotpoint	Maytag
Nominal dryer capacity (kg)	4	10.5
Drum diameter (m)	0.45	0.69
Drum depth (m)	0.35	0.56
Lifter height from wall (m)	0.043	0.107
Number of lifters	3	3
Lifter angle (front face to drum wall)	120°	112°
Drum rotational speed (rpm)	57	55
Drum wall Froude number, Fr	0.82	1.15

compact vented tumble dryer. These were chosen to give insight into behavior in dryers across the available range of sizes and enable investigation into the effects of scale. The dryer specifications are detailed in Table 1.

Both dryers were modified to disable the heater and stop the reverse action of the motor. This meant only ambient air entered the dryer drum, minimizing evaporation of moisture from fabrics, and enabled a pseudo steady state flow to be reached, allowing calculation of time averaged Eulerian data for both wet and dry conditions. These were investigated separately to understand how motion changes throughout the drying cycle. The drum design and rotational speed is as supplied by the manufacturer to ensure results are representative of consumer drying conditions. Experiments consisted of an equilibration period of 10 min followed by 30 min of data acquisition. Initial scoping experiments determined the tracer particle would make sufficient passes through each section of the drum in this time to assume ergodicity.

Fabric bundles were prepared to represent a range of loads used by consumers. All fabrics were 2-ply cotton ballast sheets supplied by Calderon Textiles (USA). The surface density of dry fabrics was  $526 \pm 1 \text{ g m}^{-2}$ , calculated by placing samples of known surface area in an oven at  $80^\circ\text{C}$  for 4 h. The equilibrium moisture content of the fabric was 4.8% (dry basis) when left in a climate-controlled laboratory at  $18 \pm 2^\circ\text{C}$  and  $45 \pm 5\%$  RH for 24 h. This moisture content represents 'dry' conditions. To investigate wet conditions fabrics were soaked in water for 30 min then spun dry in a White Knight 28009 W Gravity Drain Spin Dryer, emulating the rinse and spin cycles of a domestic washing machine. The bundle was weighed before soaking and after spin drying to ensure a moisture content of  $40 \pm 2\%$  (dry basis) was achieved, henceforth referred to as 'wet' conditions. This is typical of fabric moisture content following washing under consumer representative conditions. Over the course of the experiment minimal evaporation occurred, with the moisture content falling no more than 3%.

For the larger dryer, dry fabric bundle sizes of 2 kg, 4.5 kg, and 7 kg were used. Each fabric sheet was  $0.50 \times 0.50 \text{ m}^2$ . Initial experiments suggested the effect of fabric size was minimal compared to the impact of load size or moisture content, so was deemed beyond the scope of this study. For the smaller dryer 0.5 kg, 1.25 kg, and 2 kg fabric bundles were used, which represents equivalent volumetric fill ratios to the larger dryer assuming the change in packing density due to height variations is negligible. The fabrics used for the smaller dryer were  $0.33 \times 0.33 \text{ m}^2$ , representing the same fabric length to dryer diameter ratio as those used for the larger dryer. All bundle weights were within  $\pm 0.1 \text{ kg}$  and fabric sheets were within  $\pm 0.01 \text{ m}$  of the stated values. As it is not possible to measure the volume occupied by fabrics during drying, load sizes have been specified by dry fabric weight. The volumetric fill level in the drum is proportional to load weight assuming there is negligible increase in compression for larger loads.

The coefficient of friction between the fabrics and a stainless steel sheet representative of the drum wall material was recorded using a ForceBoard friction tester under ambient conditions with wet and dry fabrics prepared as described above. A vertical load of  $1.5 \pm 0.4 \text{ N}$  was applied to each fabric sample, and the relative velocity between the fabric sample and stainless steel surface was set to  $10 \text{ mm/s}$ . Measurements were repeated 10 times with 3 separate samples for each set of conditions.

A single 4 mm glass bead tracer particle weighing  $0.082 \pm 0.002 \text{ g}$  was glued to the center of one fabric sheet in each PEPT experiment. Figure 3 shows the tracer particle attachment location and resultant LoRs. The location of the tracer was considered an average for the whole sheet; however, this method excludes understanding of deformation and the behavior of the fabric edges. To give insight into these, additional experiments were carried out with the tracer at the corner of a fabric sheet. Experiments also studied a tracer particle attached to the center of an article representing a dryer sheet; a spun bonded PET substrate measuring  $0.15 \times 0.23 \pm 0.005 \text{ m}^2$  and weighing  $2.2 \pm 0.05 \text{ g}$ . Sheets with no SFE were used to ensure constant mass. The surface density of the sheet was  $63.8 \pm 0.5 \text{ g m}^{-2}$ , much lower than that of the fabric items. Final experiments were carried out using a wool 'dryer ball' with a tracer glued inside a small surface incision. This spherical ball had a diameter of  $7.5 \pm 0.5 \text{ cm}$  and mass of  $50.3 \pm 2.0 \text{ g}$ . The mass of the tracer particle was small compared to that of the

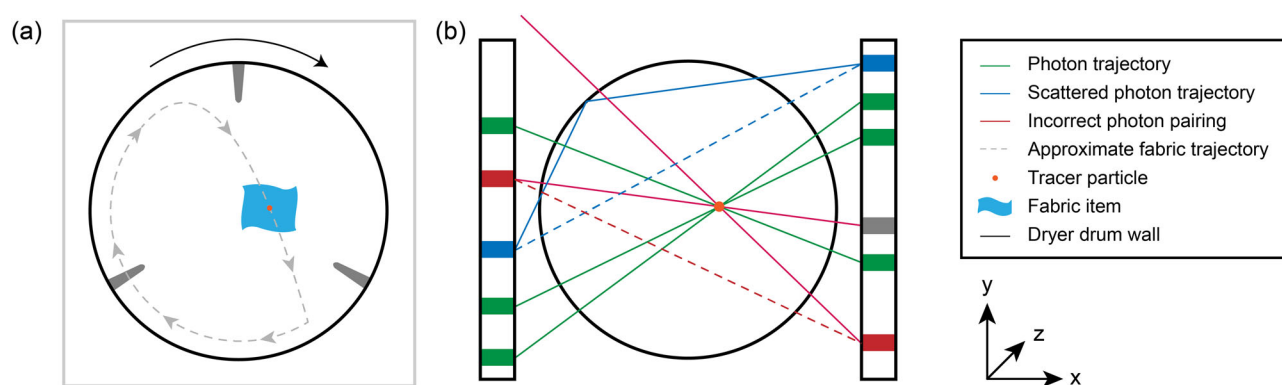


**Figure 3.** Schematic representation of (a) a tracer particle attached to a fabric sheet tumbling in a dryer and (b) lines of response from the tracer particle to the PEPT detector heads.

fabric, dryer sheet and wool ball, so had minimal effect on their motion.

## 2.1. Data processing and analysis

The PEPT-ML tracking algorithm outputs time-stamped Cartesian  $x$ ,  $y$ ,  $z$  coordinates. Each data set was analyzed using purpose written scripts in MATLAB R2019b, available upon request. The tracer locations are first transposed to align the center of the dryer drum with the origin.

### 2.1.1. Tracer velocity and acceleration

Due to the inherent noise in PEPT data, a simple two-point differentiation method (i.e., distance divided by time for successive points) yields velocity estimates with a high error. To overcome this a 2nd order polynomial can be fitted to a series of data points as a function of time using the least squares method, following the method used by Mac Namara et al.<sup>[22]</sup>

### 2.1.2. Eulerian profiles

Analysis of individual Lagrangian trajectories is difficult so to understand overall fabric motion these were converted to Eulerian flow fields. A two-dimensional radial projection of the dryer drum was divided into a grid of square cells, each measuring 0.01 times the drum radius. An  $x \times y$  grid was used as it was anticipated there would be limited motion in the axial,  $z$ , direction.<sup>[12]</sup> For this grid size a tracer particle in a 1.25 kg load of dry fabrics in the small dryer entered each cell on average  $60.9 \pm 34.2$  times in a 30 min experiment, allowing accurate calculation of time averaged values. Velocity, acceleration, and occupancy, defined as the time spent in each cell as a fraction of the total experimental time, were calculated as in Mac Namara et al.<sup>[22]</sup>

For the large dryer, it was only possible to fit half of the total height within the PEPT camera field of view at any one time. As such, data was recorded for the top and bottom halves of the drum separately, with comparable conditions maintained across repeat experiments. Lagrangian analysis of the tracer trajectories was carried out individually for each repeat experiment. These were converted to Eulerian profiles for each half of the drum and the two plots combined to produce the full flow field.

The percentage difference in Eulerian velocity between the same cell in two separate experiments was found by calculating the difference between the velocity in the two experiments, divided by the velocity from the first experiment. This can be carried out over the whole drum, and the mean and standard deviation of these percentage differences found.

### 2.1.3. Axial and radial displacement

Time averaged velocity, acceleration, and occupancy profiles are useful to understand the bulk behavior of fabrics and delivery articles. However, they give little insight into the degree of mixing in the dryer. Effective mixing is required to ensure the delivery article deposits SFE uniformly over the full surface area of the fabric load. Insight into this behavior can be gained by considering the change in axial and radial position of the tracer during each rotation. The location of the tracer was recorded each time the particle passed upwards across the horizontal center line of the drum, i.e., a full rotation was completed. For each pass the average axial coordinate and radius were calculated and subtracted from the average values of the previous pass, and data fitted to a probability density function using a kernel density estimation. The MATLAB R2019b 'ksdensity' function with a normal kernel smoother was used to calculate estimates, with the optimal bandwidth for a normal density

estimation calculated, as described by Bowman and Azzalini.<sup>[25]</sup> As a continuous tracer trajectory could not be recorded for the large dryer, this analysis was only possible for the smaller dryer.

#### 2.1.4. Effective Froude number

Froude number, as discussed in section 2.1, is a useful indicator of behavior in rotating drums. However, the Froude number for the drum wall may not correspond to the behavior of the fill media due to differences in radial position and velocity. For example, the linear velocity required to induce centrifugation decreases as distance from the drum wall increases. An effective Froude number for a tracer particle attached to an item within the drum,  $Fr_{\text{tracer}}$ , can be calculated using measured radius, i.e., the distance between the tracer and center of the drum and velocity. Assuming the tracer particle position is a good representation of the center of mass, the Froude number for the attached fabric or delivery article can be defined as shown in Eq. (1).

$$Fr_{\text{item}} \approx Fr_{\text{tracer}} = \frac{\omega_{\text{tracer}}^2 R_{\text{tracer}}}{g} = \frac{v_{\text{tracer}}^2}{R_{\text{tracer}} g} \quad (1)$$

Centrifugation will occur when centripetal and gravitational forces are in balance, i.e.,  $Fr = 1$ .<sup>[26]</sup>

### 3. Results and discussion

#### 3.1. Validation of the PEPT method

To test the accuracy of the PEPT equipment and PEPT-ML algorithm, a tracer particle was attached to the inside drum wall at a known location and the drum rotated for 10 cycles. In this time 26,714 data points were recorded and the mean deviation between the measured and actual location was 5.39 mm in the

$x$ -direction, 3.11 mm in the  $y$ -direction and 3.50 mm in the  $z$ -direction. The standard deviation of measured coordinates for a tracer particle held stationary at the center of the dryer drum for 60 s was 1.05 mm in the  $x$ -direction, 0.44 mm in the  $y$ -direction and 0.42 mm in the  $z$ -direction. This shows a high degree of accuracy for a stationary tracer, with increased noise when in motion. This has been accounted for in this analysis using the polynomial fitting method discussed in section 3.1.1. The accuracy here is less than achieved by Nicușan and Windows-Yule<sup>[23]</sup> due to the high density of the dryer wall material. The accuracy achieved is of the same order of magnitude as the tracer particle diameter, sufficient to calculate highly accurate tracer trajectories.

#### 3.2. Motion of fabrics

Figure 4 shows example tracer trajectories in the small dryer drum from (a) front on as if looking through the dryer door and (b) side on as if looking through the right side wall. The paths shown demonstrate the range of trajectories seen while transitioning through the cascading, cataracting, and centrifuging regimes, and are typical of behavior in both dryers. While some noise can be observed in the tracer paths, the overall motion is smooth suggesting little rotation of the fabric sheet with the tracer attached to the center. If the item was twisting or deforming the trajectories would be expected to show oscillatory motion.<sup>[22]</sup> Figure 4(c) shows a velocity flow field for a standard load of fabrics in the small dryer, indicating the direction of travel and magnitude of velocity at each location.

By examining the individual trajectories and overall flow field, motion can be categorized into 6 regimes. Approximate locations where these are observed are overlaid on the flow field shown in Figure 4(c).

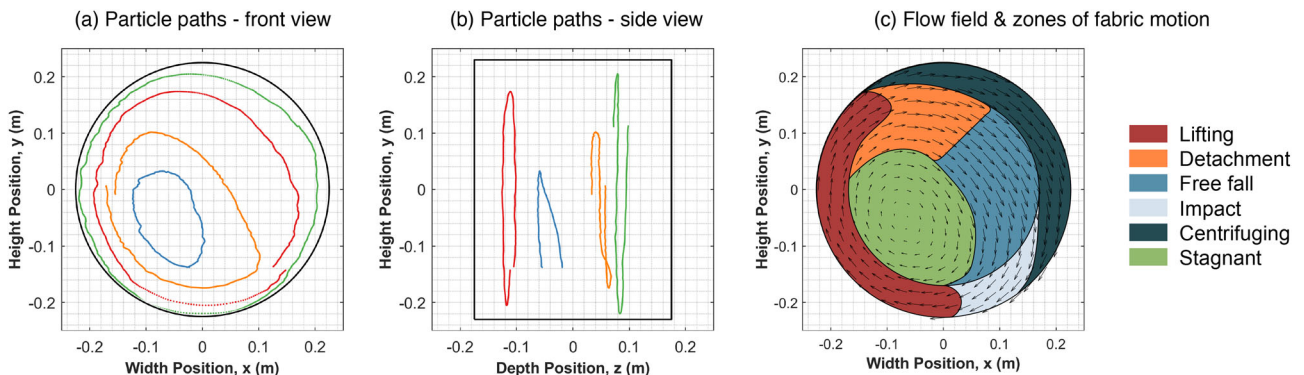


**Figure 4.** Individual tracer trajectories in the small dryer in the (a)  $x$ - $y$  and (b)  $z$ - $y$  planes, and (c) a velocity flow field for a 1.25 kg load of dry,  $0.33 \times 0.33 \text{ m}^2$  fabrics in the small dryer with identified regions of motion shown.



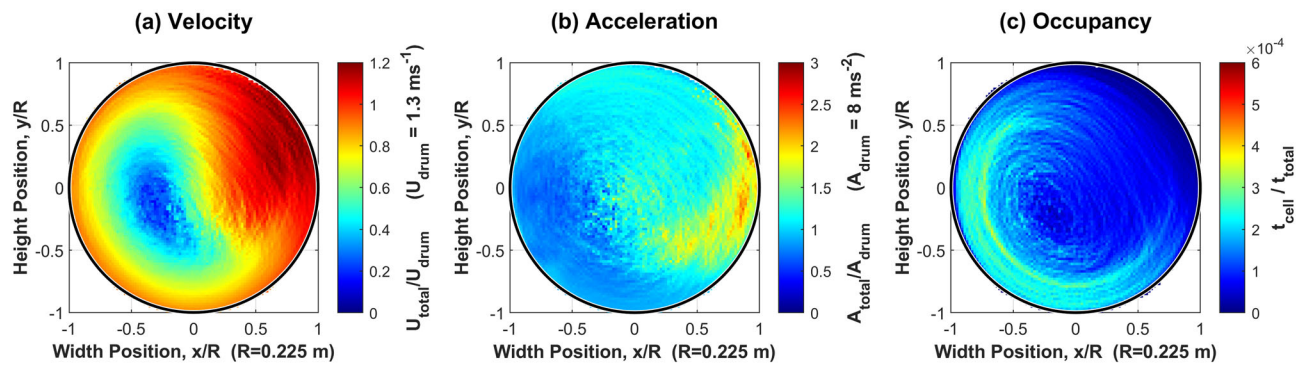


**Figure 5.** Eulerian velocity, acceleration and occupancy profiles, normalized against the equivalent values for the drum wall, for a tracer particle attached to the center of a fabric sheet in a 1.25 kg load of dry,  $0.33 \times 0.33 \text{ m}^2$  fabrics in the small dryer.

- In the *lifting region* fabrics follow a circular trajectory near the drum wall, forming a compressed bed.
- In the upper left of the drum trajectories *detach* from the wall. The centrifugal forces imparted on the fabric from the drum are overcome by gravity and the fabric begins accelerating downwards.<sup>[15]</sup> Detachment location is strongly related to lifting radius, with those closest to the drum wall generally detaching last as centrifugal forces are largest.
- Most fabrics then *free fall* through the disperse region in a cataracting motion ( $Fr < 1$ ), as described in section 2.1, before impacting the fabric bed below.
- The items which detach last will often follow a higher trajectory, with some moving toward the *centrifuging* regime ( $Fr \geq 1$ ); i.e. they remain close to the drum wall and form the base of the fabric bed on their next rotation, tending to directly impact the drum wall rather than the bed of fabrics.
- Fabrics traveling further than 0.08 m from the drum wall have little kinetic energy and may detach very early, entering the slow-moving *stagnant zone* close to the center of rotation ( $-0.077, -0.027$  in Figure 4(c)) in the lower left quadrant.

The lifting action of the drum was seen to extend past the lifter tip radius, suggesting lifting is determined by a combination of fabric-wall, fabric-lifter, and fabric-fabric interactions. Comparing the radial and axial views in Figure 4(a,b) shows motion is primarily two-dimensional, with much less forward and backward movement.

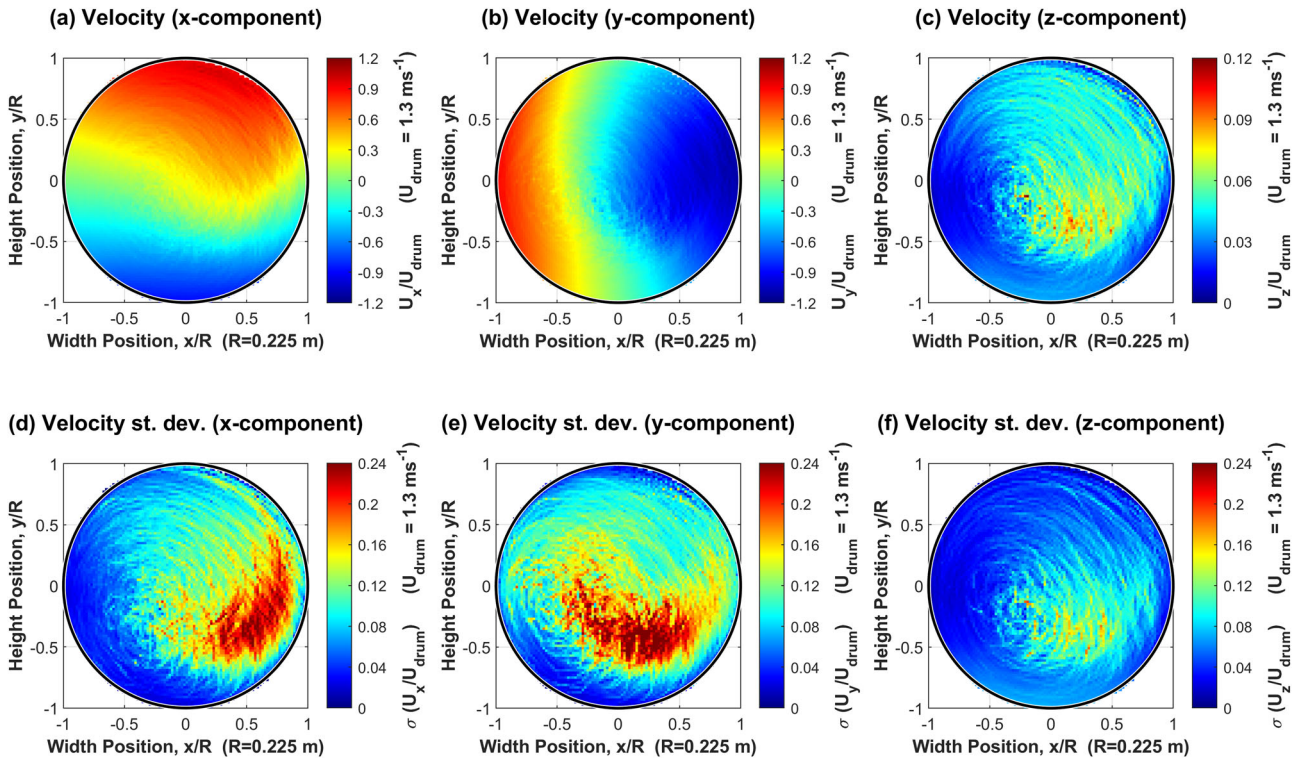
### 3.3. Fabric velocity and acceleration

Figure 5 shows the Eulerian velocity, acceleration and occupancy profiles for a tracer attached to the center

of a fabric sheet in the 1.25 kg dry load experiment using the small dryer. For these plots, position, velocity and acceleration are given as a fraction of the equivalent value for the dryer drum wall, represented by the black circle. In the following, data will be presented from the small dryer drum, with differences between the two drum sizes discussed in section 4.5.1.

During lifting, fabrics in direct contact with the drum wall had a tracer velocity close to the drum rotational speed. Fabrics here are strongly influenced by the drum wall with frictional forces between the two pulling fabrics upwards, aided by the motion of the lifters. Some slipping occurs, leading to the slightly lower velocity of fabrics compared to the drum. For passes of the tracer further from the wall the velocity was lower, falling linearly from a radius of  $R$  (i.e., in contact with the drum wall) to  $0.4 R$  in the lifting region. Some decrease is expected due to the change in rotational speed with radius. However, the observed reduction in the lifting region is much greater than would be seen if fabrics were rotating as a solid body. Along the horizontal center line, the mean tracer velocity at the wall was 87.9% of the drum rotational speed, falling to 60.2% of the equivalent rotational speed ( $U = r \times \omega$ ) at  $r = 0.4 R$ . The lifting action of the drum appears less as the radius decreases due to reduced wall-fabric interactions, with fabric reliant on frictional forces with other items for lifting. The resulting shearing action between layers of fabric will likely have significant implications for SFE delivery. The tracer velocity was consistent throughout the height of the lifting region for a given radius and increasing angular coordinate, with the Eulerian velocities in the cells along a radius of  $0.9 R$  having a standard deviation of 0.0124.

Figure 6(a-c) shows the  $x$ ,  $y$ , and  $z$  components of velocity that make up the profile of Figure 5(a), giving additional insight into the travel of the tracer particle. As expected, velocity in the  $x$ -direction is positive in



**Figure 6.** Eulerian velocity and velocity standard deviation profiles, normalized against the drum wall velocity, in the  $x$ ,  $y$ , and  $z$ -directions for a tracer particle attached the center of a fabric sheet in a 1.25 kg load of dry,  $0.33 \times 0.33 \text{ m}^2$  fabrics in the small dryer.

the top half of the drum as the tracer moves from left to right, and negative in the bottom half as it moves back to the left. The same phenomenon is observed in the  $y$ -velocity profile as the tracer moves up with a positive velocity and down with a negative velocity, in line with the direction of travel of the drum wall. As the tracer approaches its highest point, the  $y$ -component of velocity shown in Figure 6(b) begins to decrease as the fabric accelerates downwards in the detachment segment. Fabric trajectories transition from a circular path in the lifting region to a downwards parabola in the free fall zone, as shown in Figure 4. Here the fabric is no longer in contact with the drum wall, with behavior instead determined by fabric collisions and gravity. The  $x$ -component of velocity falls slowly as it is only influenced by fabric–fabric interactions here, while the  $y$ -component increases rapidly to a maximum, as shown in Figure 6. When the fabric impacts the drum wall or fabric bed below, its velocity increases in the  $x$ -direction while slowing in the  $y$ -direction, until its trajectory returns to the upwards circular path through the lifting zone.

Axial motion is much slower than radial movement. As such the scale for the  $z$ -component of velocity has been reduced by an order of magnitude. In the lifting region there is no significant motion in the

axial direction as fabrics are held against the wall in a compressed bed. The  $z$ -component of velocity increases through the detachment and falling regions to a maximum in the impact zone.

Figure 6(d–f) shows the standard deviation of velocity in each cell for the  $x$ ,  $y$ , and  $z$ -directions. The velocity range is lowest in the lifting and detachment regions, where fabrics are in a packed bed pressed against the drum wall, with little relative motion between items. The standard deviation in the  $y$ -direction increases toward the top of the lifting zone and start of the detachment zone. Throughout the falling zone a standard deviation on the order of  $\pm 0.1$  times the drum rotational speed was observed as fabric motion became independent of the drum wall. Behavior during falling is influenced by detachment conditions and interactions with other items, leading to a wide range of velocities. This increases to a maximum in the impact region, where the standard deviation reaches a maximum of  $\pm 0.24$  times the drum rotational speed. The complex nature of collisions with other fabrics and acceleration into the lifting zone leads to significant variability, suggesting a shearing action is present in the impact zone. Less variation is observed in the centrifuging region. Figure 6(f) shows little variability in the  $z$ -direction

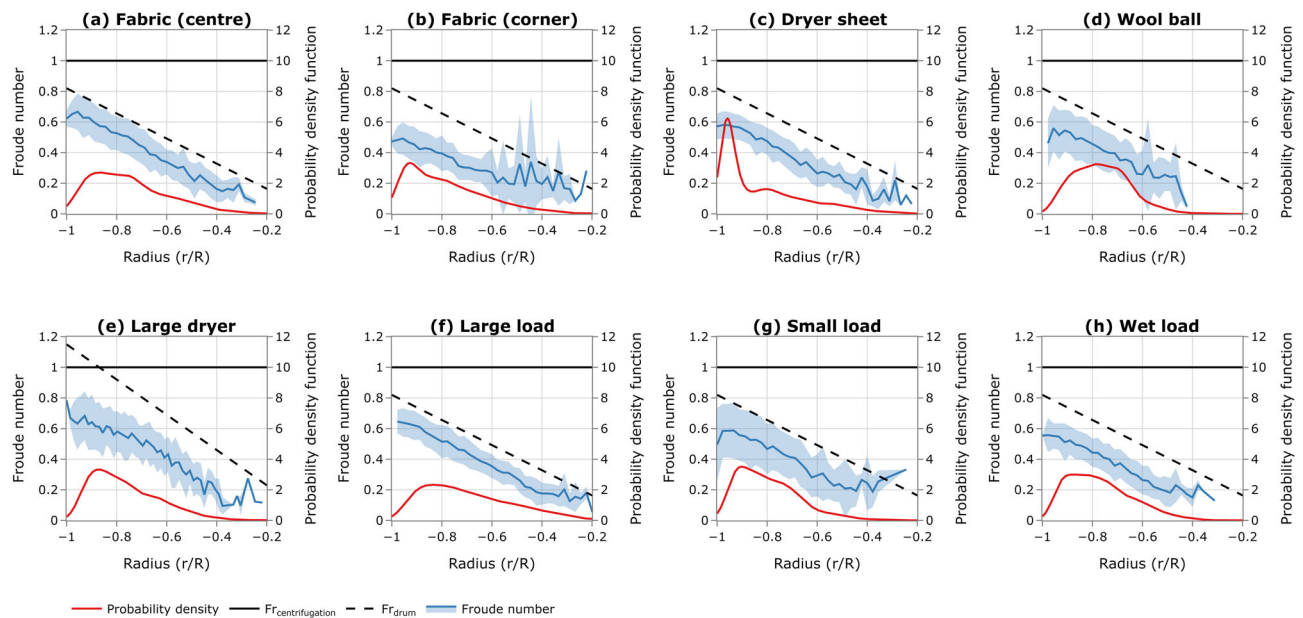


**Figure 7.** Calculated Froude number (Eq. 1) versus radius for a tracer particle passing the horizontal axis for (a) a fabric (center), (b) fabric (corner), (c) dryer sheet, and (d) wool ball in a 1.25 kg dry load in the small dryer and a fabric (center) in a (e) 4.5 kg dry load in the large dryer, (f) 2 kg dry load in the small dryer, (g) 0.5 kg dry load in the small dryer and (h) 1.25 kg wet load in the small dryer, with the Froude number for centrifugation, drum angular velocity (Eq. 5) and probability density function for the radius of passes shown.

throughout the lifting, detachment and centrifuging zones. This increases in the falling region to a maximum upon impact. The range of velocities observed in the impact region suggest this is key for mixing in the axial direction. This is important for SFE delivery and will be explored further in section 4.7.

### 3.4. Tracer froude number

Figure 7 shows the Froude number (Eq. 1) versus radius for a tracer particle passing the horizontal axis, along with the Froude number required for centrifugation ( $Fr = 1$ )<sup>[26]</sup> and expected value for the drum wall angular velocity, at a number of operating conditions. Note all subplots represent conditions in the small dryer, except Figure 7(e). A probability density function for the number of passes at each radius, calculated as described in section 3.1.3, is also shown. The Froude number calculated at this point is a good representation of the overall behavior throughout the height of the lifting zone, and will determine behavior as the tracer transitions through the centrifugation or falling and impact regions. Figure 7(a) shows the values for a tracer particle attached to the center of a fabric sheet in a dry, 1.25 kg load in the small dryer. The highest values observed are close to that of the drum, clearly showing the influence of the wall and lifters in this region. The amount of wall slip varies, giving a range of Froude numbers observed at a single

radius. This is likely due to the varying influence of the lifters, with some passes falling in the gaps between these and interacting with them less. The mean Froude number along the horizontal line ranges from 0.63 at the wall to a minimum of 0.16 at the boundary with the stagnant core. These values are consistently below the equivalent for the drum, which ranges from 0.82 at the wall to 0.33 at a radius of  $0.4 R$ , and are also below  $Fr = 1$ , i.e., the value required for centrifugation. However, some centrifugation was observed, with the occupancy profile in Figure 5(c) showing passes through all regions of the drum. This is due to acceleration in the detachment region, shown in Figure 5(b), which increases the Froude number of fabrics closest to the wall above  $Fr = 1$ . As expected, a tracer closer to the wall has a higher  $Fr$ , resulting in later detachment and cataracting behavior. This falls with radius and transitions to cascading behavior as the tracer approaches the stagnant core. The probability density function shows the highest proportion of passes are between a radius of  $0.75 R$  and  $0.9 R$ , corresponding to Froude numbers of 0.49 and 0.61, respectively. A low density region is observed close to the drum wall due to the thickness of the partially folded fabric. This suspends the tracer particle away from the wall, leading to a low probability of direct tracer-wall contact. The number of passes between the dense bed region and drum center trails off as the radius decreases, down to zero at  $0.24 R$ .



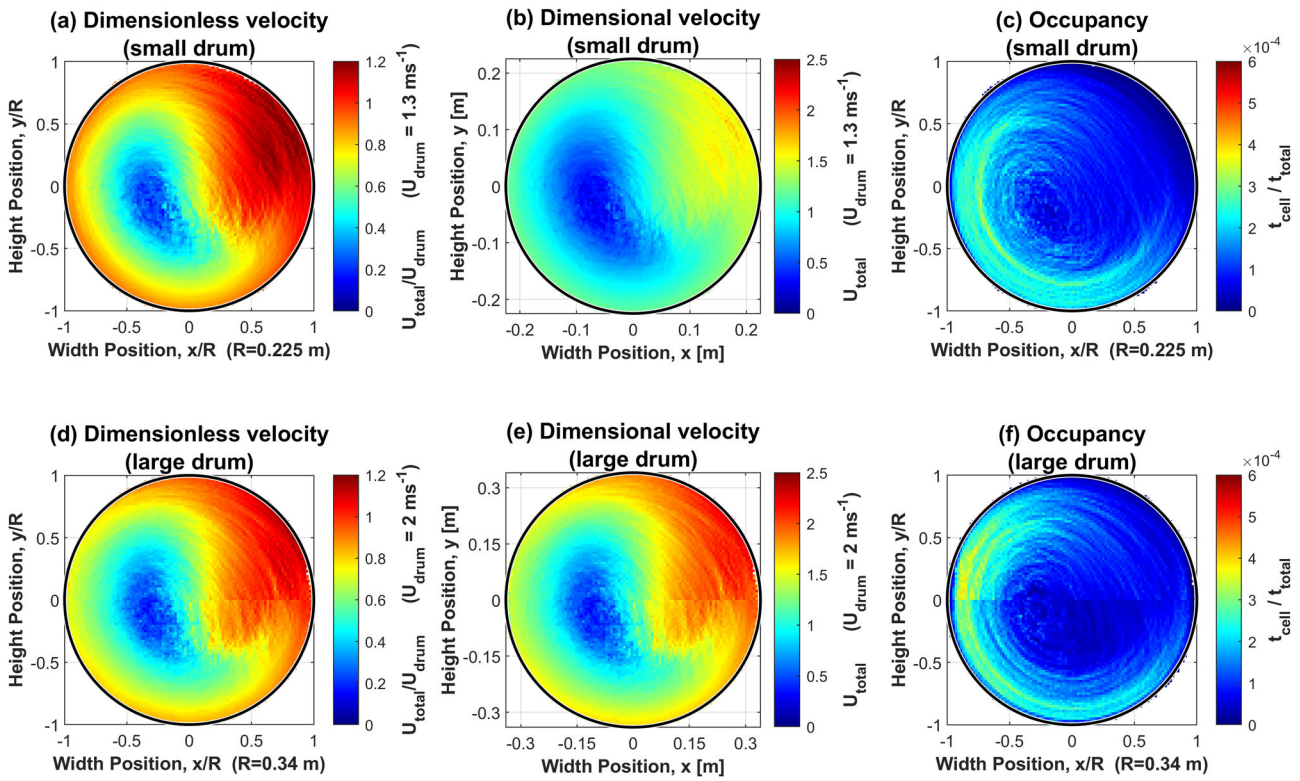


**Figure 8.** Eulerian dimensionless velocity, dimensional velocity and occupancy profiles for a tracer particle attached the center of a fabric sheet in (a–c) a 1.25 kg load of dry,  $0.33 \times 0.33 \text{ m}^2$  fabrics in the small dryer and (d–f) a 4.5 kg load of dry,  $0.5 \times 0.5 \text{ m}^2$  fabrics in the large dryer.

The Froude number at this position is close to 0.1, at which behavior transitions from the cataracting to cascading regime.<sup>[8]</sup>

### 3.5. Effect of drying conditions

#### 3.5.1. Effect of dryer size

Figure 8 shows velocity and occupancy profiles, for the small and large dryer. The dimensionless velocity values in plots (a) and (d) have been calculated by dividing the measured velocity by the drum wall velocity. Comparing plots (b) and (e) shows the *absolute velocity* in the two dryers is quite different. Much higher speeds are reached in the lifting and falling regions for the large dryer due to the higher drum wall rotational speed and free fall distance, with calculated Eulerian velocities  $33.0 \pm 10.7\%$  above those in the small drum. However, when the same data is presented as a *fraction of the drum wall velocity* in plots (a) and (d), behavior is seen to be similar. Dimensionless velocities in the large dryer were on average 8.5% lower than the small dryer with a standard deviation of 7.9%, likely due to increased slipping in the lifting zone. The occupancy profile shows a thinner fabric bed in the larger dryer, with fabrics in this region spending more time close to the drum

wall. Cells in the bed typically have an occupancy value above  $2 \times 10^{-4}$ . In the lower left quadrant of the drum 42.3% of cells in the small drum and 29.2% of cells in the large drum were above this threshold, for equivalent load sizes. For the same region the total occupancies were similar, 34.3% for the small drum and 31.0% for the large drum. This suggests fabrics occupy a smaller fractional volume close to the drum wall in the larger drum, increasing their average radius during lifting and leading to later detachment, with behavior closer to centrifugation.

The difference in Froude number between the two dryers,  $Fr = 0.82$  for the small drum and  $Fr = 1.15$  for the large drum, suggests behavior for an identical fill media would transition through the flow regimes shown in Figure 2, toward centrifuging behavior.<sup>[8]</sup> This is in line with the thinner bed and higher Froude number observed in Figure 7(c), resulting in later detachment in the larger dryer. The mean tracer  $Fr$  observed in the larger dryer ranged from 0.78 at the wall to a minimum of 0.10. While higher than those observed for the small dryer, this range is still in the cataracting regime. The small amount of centrifugation occurring is likely due to acceleration in the subsequent detachment region. In the upper right quadrant of the drum the proportion of time

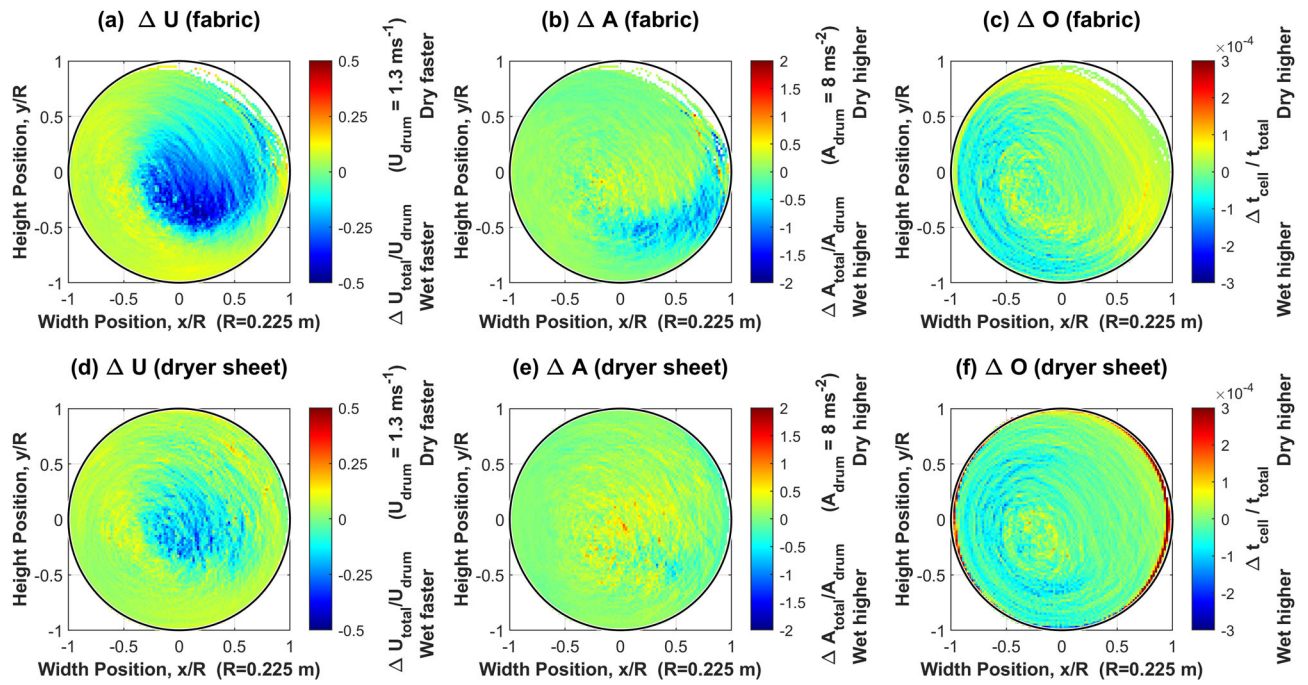


**Figure 9.** Difference in Eulerian velocity, acceleration and occupancy profile, normalized against the equivalent values for the drum wall, between a wet and dry load of fabrics for a tracer particle attached to (a–c) the center of a fabric sheet and (d–f) a dryer sheet in a 1.25 kg load of  $0.33 \times 0.33 \text{ m}^2$  fabrics in the small dryer.

spent within  $0.1 R$  of the drum wall (i.e., trajectories following a centrifuging path adjacent to the wall) fell from 1.1% of experimental time for the large drum to 0.4% for the small drum. When operating at a constant volumetric fill level and characteristic length, behavior is predicted well by drum Froude number. However, other factors are also involved, such as lifter design and drum wall friction, which have not been examined in this work.

### 3.5.2. Effect of fabric moisture content

A number of operating conditions may influence fabric and delivery article motion in the dryer. The aim of drying is to reduce the moisture content of fabrics to their equilibrium level. As such the process is dynamic, with a constantly decreasing moisture content that reduces the load mass and will change surface properties including friction coefficients. To maintain steady state conditions the behavior of wet and dry fabric loads was investigated separately. The difference in velocity, acceleration and occupancy between a wet and dry load is shown for a tracer particle attached to the center of a fabric item and dryer sheet in Figure 9. The profiles show the wet value subtracted from the dry value (i.e., that shown in Figure 5 above), with negative (blue in the figure) results suggesting a higher value for wet conditions and vice versa for positive results.

Dry fabrics traveled  $9.9 \pm 3.9\%$  faster than wet fabrics in the lower left quadrant between  $R$  and  $0.6 R$ . The fraction of experimental time for the same region increased from 26.8% for dry fabrics to 32.9% under wet conditions. The lower velocity and higher occupancy seen for wet fabrics during lifting are caused by increased slipping at the wall, resulting in the lower  $Fr$  seen in Figure 7(h), perhaps due to changes in the friction coefficient and structural changes to the fabrics. Wet fabrics were seen to detach from the wall and begin falling earlier, reducing the size of the stagnant zone, as shown in Figure 9(a). Swelling of the dual pore fabric structure when saturated with water reduces deformability and leads to each fabric balling up around its center of gravity.<sup>[22]</sup> As moisture content falls the fabric structure becomes more open. In the spherical geometry observed under wet conditions the center of mass of the fabric plug is further from the drum wall, as seen by the reduced number of passes adjacent to the wall in Figure 7(h). At this reduced radius, the tracer Froude number is lower. The spherical geometry also has a much lower surface area available for lifting. This effect overcomes the increase in friction coefficient, from  $0.181 \pm 0.004$  for dry fabrics to  $0.424 \pm 0.003$  for wet fabrics, calculated as described in Section 3. The reduction in Froude number reduces centrifugation, as can be seen in the occupancy profile in Figure 9(c), with no passes adjacent to the wall shown in the upper right quadrant.



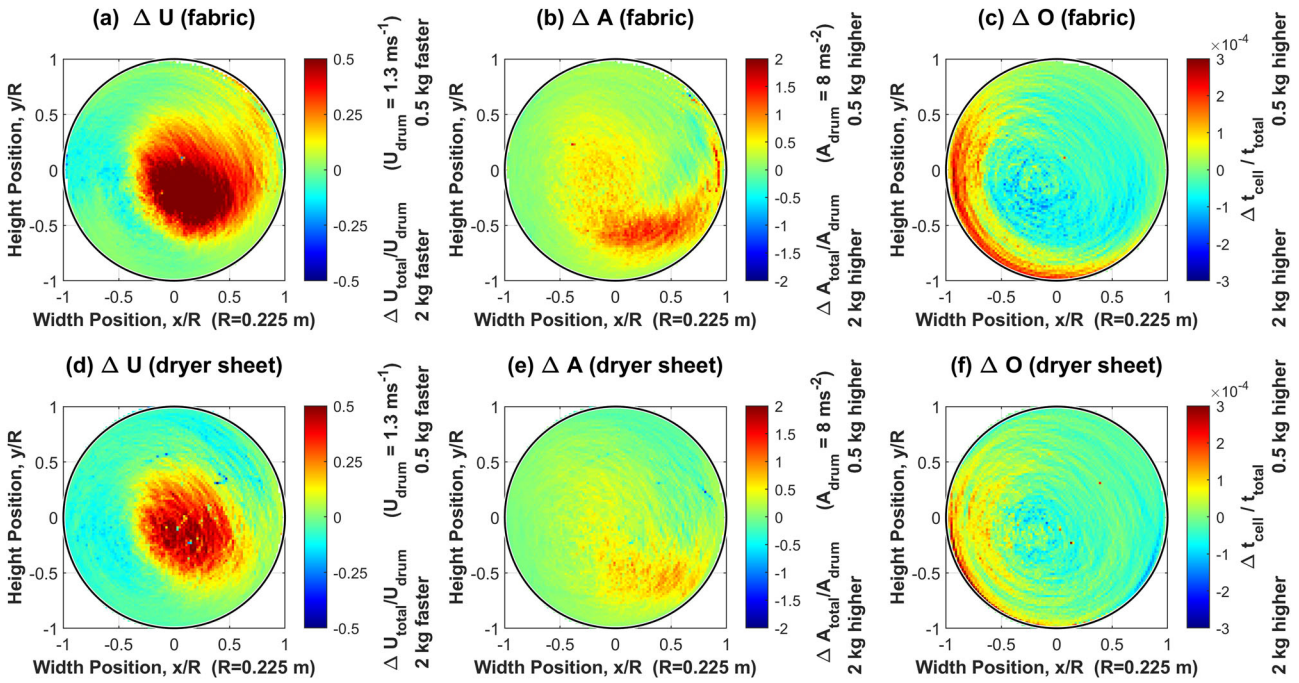


**Figure 10.** Difference in Eulerian velocity, acceleration and occupancy profile, normalized against the equivalent values for the drum wall, between a 2 and 0.5 kg load of fabrics for a tracer particle attached to (a–c) the center of a fabric sheet and (d–f) a dryer sheet in a dry load of  $0.33 \times 0.33 \text{ m}^2$  fabrics in the small dryer.

However, the free fall velocity of wet fabrics increased significantly, with impacting items traveling up to  $0.70 \text{ m s}^{-1}$  faster than the dry equivalent. This caused a higher deceleration upon impact which could increase fabric wear. The higher speeds observed under wet conditions are due to the same structural differences between wet and dry fabrics. The spherical structure of wet fabrics reduce interaction with other items. Under dry conditions the higher fabric surface area available increases fabric–fabric interactions, dampening its initial acceleration.

### 3.5.3. Effect of load size

The most significant condition to influence behavior in the dryer was load size. Figure 10 shows the difference in velocity, acceleration and occupancy between a 0.5 and 2 kg load for both a fabric item and dryer sheet. A positive (red) result indicates a higher value was observed for the 0.5 kg load than the 2 kg load, and vice versa for a negative (blue) result. The velocity profile in Figure 10(a) shows no significant changes in the lifting and detachment zones. However, as the fill level increases the fabric bed in the lifting region grows, as shown in Figure 10(c). Fabrics are more likely to be further from the wall in the stagnant core, traveling at a much lower velocity. This can be seen in Figure 7(f,g) where the number of passes drops sharply between  $0.7 R$  and  $0.8 R$  for the small load, compared to a more gradual decline for the larger

load. Fabrics are more frequently close to the drum wall in the small load, with a higher  $Fr$  and later detachment point. Items that are lifted up to the detachment zone in the large load fall onto those in the core region below, obstructing their path and resulting in slower observed velocities in the falling region. Conversely, in the smaller load fabrics could move around without interacting with other items and reached significantly higher velocities when falling. The mean velocity in the upper right quadrant of the drum was  $14.7 \pm 12.4\%$  higher for the 0.5 kg load than the 2 kg load. This causes considerable deceleration upon impact which may again influence fabric wear.

## 3.6. Fabric and delivery article behavior

### 3.6.1. Tracer particle location $\Delta$ fabric sheets

For the majority of experiments the tracer particle was attached to the center of a fabric sheet. This was assumed to represent the center of mass and give an average location for the overall fabric sheet. However, this location does not give a full insight into behavior at the fabric edges. Mac Namara et al.<sup>[22]</sup> considered fabric items as spherical plugs, but here individual fabrics in the dryer had an open structure. As such deformation can occur over the total fabric area. Figure 11 compares velocity, acceleration and occupancy profiles for tracers attached to the center and

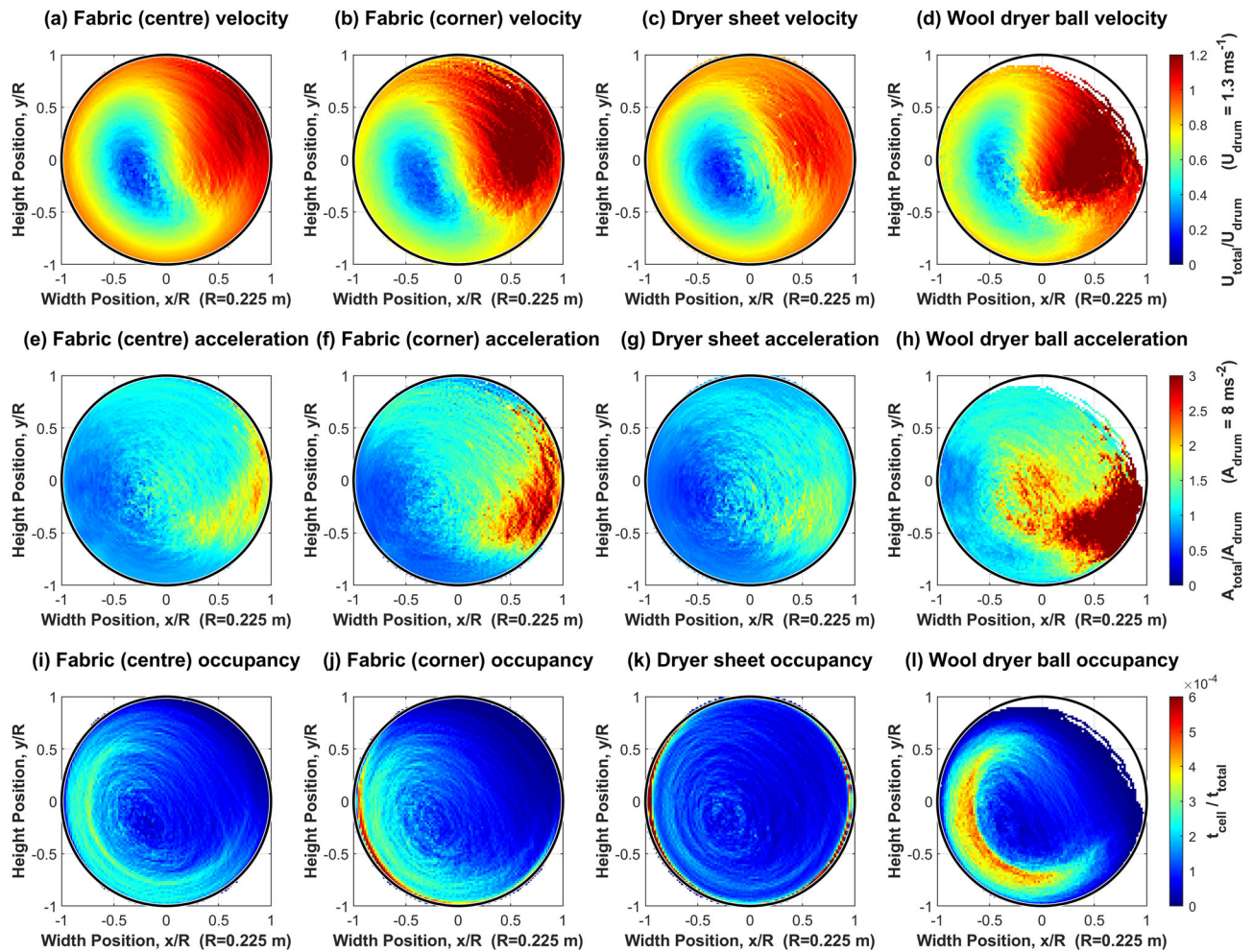


**Figure 11.** Eulerian velocity, acceleration and occupancy profiles, normalized against the equivalent values for the drum wall, for a tracer particle attached to the center of a fabric sheet, the corner of a fabric sheet, a dryer sheet and a wool dryer ball in a 1.25 kg load of dry,  $0.33 \times 0.33 \text{ m}^2$  fabrics in the small dryer.

corner of a fabric item. In the lifting region the velocity of the center tracer was higher, an increase of  $21.8 \pm 5.0\%$  over the corner tracer observed in the lower left quadrant between  $R$  and  $0.6 R$ . This is in line with observations in section 4.3 that behavior here depends on frictional interactions between the drum wall and fabric. The corner tracer spent more time at the base of the fabric bed, adjacent to drum wall in the lifting zone. The radius here is determined in the impact region, where fabric extremes are often flung out toward the drum wall during the free fall phase. When falling through the upper right quadrant between the center and a radius of  $0.9 R$ , the fabric corner reached speeds on average  $13.5 \pm 9.2\%$  higher than at the fabric center. The higher falling speed causes a corresponding increase in deceleration in the impact region, reaching values  $22.9 \pm 25.2\%$  higher for the corner tracer in the lower right quadrant. This will likely lead to differences in fabric wear and SFE delivery across the fabric area.

### 3.6.2. Dryer sheet motion

Despite the large difference in surface area and mass between fabrics and dryer sheets, the velocity and acceleration profiles shown for the two in Figure 11 are similar, with the overall behavior of the dryer sheet the same as described for a fabric in section 4.2. The similarities to the motion seen for fabrics suggests interactions between the two are key in dryer sheet motion, with frictional forces dragging the sheet from its expected path. The dryer sheet was found in all regions of the drum, as shown by the occupancy profile in Figure 11(k) where a white cell would indicate no passes by the tracer. However, the majority of time was still spent adjacent to the wall, with key differences to the profiles shown for fabrics in Figure 11(i,j). The dryer sheet spent 44.7% of time within  $0.1 R$  of the drum wall, compared to 17.7% for the fabric center tracer. The dryer sheet was marginally slower than the fabric in the lifting and detachment regions, likely due to the reduced surface area available to interact

with the wall, as observed for fabric edges. The thin geometry of the dryer sheet also allowed the tracer to get closer to the drum wall than fabric. While the mean  $Fr$  for a dryer sheet was lower than a fabric at the same radius, a high proportion of passes were closer to the wall and hence at higher Froude number. While only a small proportion of passes followed a centrifuging path for the full cycle, the high lifting  $Fr$  and acceleration in the detachment zone results in dryer sheets impacting the drum in the upper right quadrant, as shown by the high occupancy here in [Figure 11\(k\)](#).

The dryer sheet velocity was closer to that of the drum wall in the falling and centrifuging zones. The Eulerian velocities in the upper right quadrant were  $9.4 \pm 6.7\%$  lower than fabrics. Behavior is a balance between the influence of the drum wall and fabrics through friction, causing mainly centrifuging motion with some cataracting and cascading behavior. This could have significant implications for SFE delivery. If the dryer sheet is pressed against the wall, as shown occurring in [Figure 11\(k\)](#), its availability for direct SFE deposition onto fabrics is reduced. Deposition may be more prominent onto the fabric edges as these are more likely to occupy this region, shown when comparing [Figure 11\(i\)](#) and [\(j\)](#). It also increases the likelihood of secondary transfer, with the wall acting as an intermediate for transfer between dryer sheets and fabrics.

Changes to the behavior of dryer sheets under wet conditions are similar to those observed for fabrics, as shown in [Figure 9](#). Dryer sheets traveled slower in the lifting region, detaching earlier and falling  $5.8 \pm 3.8\%$  faster under wet conditions compared to the dry equivalent (in the lower left quadrant between  $R$  and  $0.6 R$ ). The fraction of experimental time spent in this zone by a dryer sheet increased from 21.8% under dry conditions to 26.5% for wet conditions. While the sheet still occasionally occupied the centrifuging region, this was much less frequent than for dry conditions. Occupancy between the drum wall and  $0.9 R$  in the upper left quadrant fell from 5.8% for a sheet under dry conditions to 1.2% under wet conditions, with the rest traveling through the main falling region, defined in [Figure 4\(c\)](#). This results in the dryer sheet impacting with the main bulk of the fabrics and mixing into the main bed more through the lifting phase, explaining the increased occupancy observed in the bulk of the lifting region discussed above. Changes in dryer sheet location throughout the drying cycle will likely influence SFE deposition mechanisms, with

more direct fabric-dryer sheet interactions occurring in the early phases.

The changes observed when increasing load size were similar for the dryer and fabrics, as shown in [Figure 10](#). As discussed, dryer sheet motion depends on that of the surrounding fabrics. The same effect was seen for both the large and small dryer when using load sizes of equal volume fraction.

### 3.6.3. Wool dryer ball motion

In contrast to the behavior of a dryer sheet, the wool 'dryer ball' showed no centrifuging behavior. The occupancy profile in [Figure 11\(l\)](#) shows no time was spent adjacent to the drum wall in the centrifuging region and very little time was spent here in the impact, lifting and detachment zones. Only 11.8% of experimental time was spent within  $0.1 R$  of the drum wall and the closest trajectory observed in the upper left quadrant was  $0.023 m$  from the drum wall. When the dryer ball did enter these regions, the observed velocity was  $10.9 \pm 2.2\%$  slower than a fabric. In the lifting region the occupancy increases throughout the height of the fabric bed to a high value close to the surface. In the lower left quadrant between  $0.6 R$  and  $0.8 R$ , i.e., the top of the bed in the lifting region, the dryer ball spent 17.8% of experimental time, compared to 11.2% for a fabric and 6.4% for a dryer sheet. However, the velocity remains below that of a fabric or dryer sheet in the same location. The increased distance from the drum wall is as expected due to the thickness of the wool ball, which reduces the radius of the center of mass. The reduced velocity during lifting results in a lower  $Fr$  than fabric at the same radius, similar to the behavior of a dryer sheet, as shown in [Figure 7\(d\)](#). However, as the ball was further from the wall than the sheet behavior was closer to the cascading regime in the detachment, falling, and impact regions. The dryer ball tends to detach much earlier than fabrics and falls close to the drum center line, resulting in the stagnant zone almost completely disappearing. The velocity reached in the falling region is higher, with values in the upper left quadrant on average  $12.9 \pm 8.8\%$  higher than those observed for fabrics. This led to large deceleration occurring upon impact, on average  $44.8 \pm 14.8\%$  higher than the equivalent for fabrics in the lower right quadrant. As discussed, its early detachment results in the dryer ball primarily occupying the top of the fabric bed upon lifting. If a similar spherical article was used for SFE delivery deposition mechanisms would vary significantly from those for dryer sheets, with the drum wall being less significant,



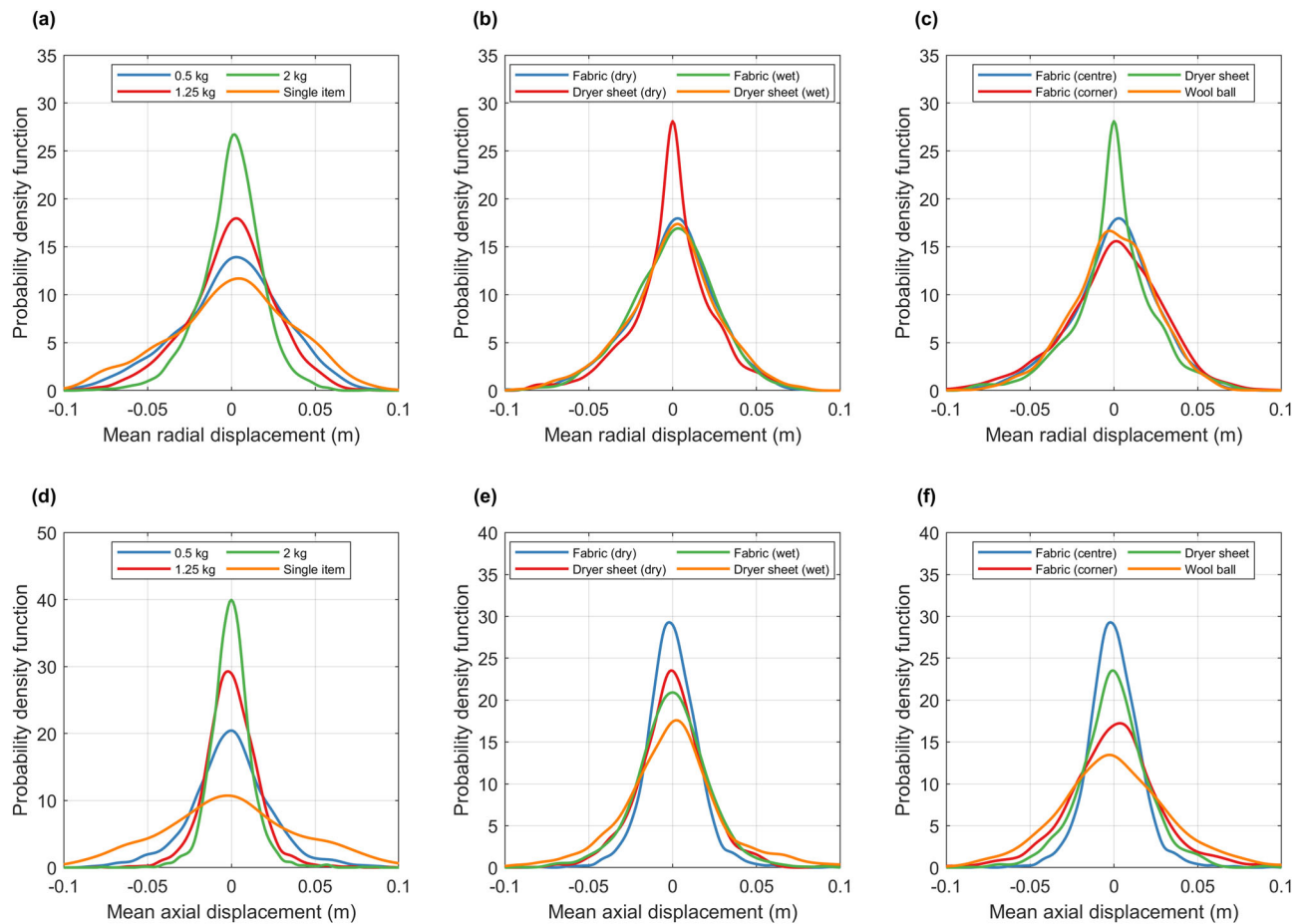


**Figure 12.** Probability density functions for the mean radial and axial displacement for (a and d) various load sizes, (b and e) moisture contents, (c and f) tracer particle locations and SFE delivery articles.

replaced by high velocity impacts and sliding at the bed surface.

### 3.7. Axial and radial displacement

Eulerian velocity, acceleration, and occupancy profiles give useful insight into the time averaged behavior in a system. However, further understanding can also be gained from examining the individual Lagrangian trajectories. Figure 12 shows probability density functions for the mean axial and radial displacement between consecutive tracer rotations. For all operating conditions investigated functions were largely symmetrical, showing an equal probability of displacement in each direction and a mean displacement of approximately zero. There was no significant correlation between displacement and mean axial and radial tracer location, except where the item could only move away from a system boundary (i.e., at the drum, front and back walls of the dryer). Figure 6(c) shows the axial velocity of a fabric sheet in the standard 1.25 kg dry load of fabrics. Axial motion in the lifting

region was limited, with the majority occurring in the stagnant core or during free fall and impact. This was observed across all experimental conditions.

The most significant difference in both axial and radial displacement occurred with load size. The highest volumetric fill ratio saw little axial or radial displacement, with the mean value for 80% of passes changing less than 3.9 mm radially and 2.3 mm axially. For the smaller 0.5 kg load, displacement increased in both directions up to 6.9 mm radially and 5.2 mm axially. As discussed in section 4.5.3, reduction in load size leaves more free space in the drum for fabrics to move. At the lowest load sizes, mixing in the drum is increased. The small changes in both axial and radial position within the drum between consecutive cycles causes a hysteresis effect, where fabrics are likely to follow similar behavior for multiple consecutive passes. Moving to conditions with higher displacement between rotations is likely to increase uniformity of SFE deposition over the fabric as the delivery article comes into contact with a higher proportion of fabrics in the drum.

Under both wet and dry condition fabrics showed similar amounts of radial displacement. Dryer sheets also showed comparable behavior under wet conditions. However, in the dry load the radial displacement observed for dryer sheets was reduced, as shown by the large central peak in Figure 12(b). This is likely due to the high proportion of time spent in the centrifuging regime, as discussed in section 4.5.2. A small increase in radial displacement was observed for a tracer particle attached to the fabric corner, compared to the fabric center. The wool dryer ball showed similar displacement to the fabrics, and much more than the dryer sheet. Fabrics showed lower axial displacement than dryer sheets, with both moving more under wet conditions. The tracer attached to the fabric corner showed significantly more axial motion than the tracer at the center. The dryer ball showed a high amount of axial movement compared to both fabrics and dryer sheets. Therefore, it is highly likely to mix well through the full fabric load. If used for SFE delivery this could significantly improve uniformity.

#### 4. Conclusions

Positron emission particle tracking has been used to give useful insight into the behavior of fabrics and SFE delivery articles in the domestic clothes dryer, under a range of operating conditions. Trajectories showed a primarily cataracting motion in a two-dimensional radial plane. The dryer drum has been separated into six regions through with the tracer particle was seen to traverse, with the majority of passes occurred sequentially through the lifting, detachment, falling and impact regions. The slowest moving items moved toward a cascading motion in a stagnant core, with the fastest tending to centrifuge. Dryer sheet behavior was seen to closely follow that of fabrics, with frictional forces between the two dominating motion of the dryer sheet. Some small differences were observed, primarily in the lifting region where dryer sheet velocities were smaller. Behavior in this zone was determined by contact area between an item and the drum wall, with an increase in available area resulting in higher velocities due to increased frictional forces and hence reduced slipping. This phenomenon was also observed when comparing behavior across the fabric sheet area, with a tracer particle attached to the corner moving slower during lifting than an equivalent at the center. The 'dryer ball' has a much lower surface area to mass ratio than the dryer

sheet or fabric, resulting in very slow velocities in the lifting region. However, much faster behavior was seen throughout the falling, impact and stagnant zones. Radius during the lifting phase was seen to determine detachment location and subsequent free fall behavior for all items. Those with a higher lifting radius were seen to detach later and reach a greater velocity when falling. This results in higher deceleration upon impact and may increase fabric wear. Dryer sheet motion was again influenced by their interactions with fabrics, with a slightly slower velocity due to slipping effects. Free fall velocity was seen to change across the fabric surface, with the corners reaching higher velocities as these were flung out from the center of gravity. Occupancy profiles showed substantial changes for different items. Fabrics spent a high proportion of time in the lifting and detachment zones, falling evenly through the free fall region. However, dryer sheets were more likely to be in direct contact with the drum wall. This is due to their more centrifuging behavior, which pushes them to the drum wall during detachment and results in them falling close to the wall, forming the base of the bed. Dryer balls showed the opposite behavior, falling early and being lifted through the top of the bed.

While drum size was seen to have a significant effect on fabric velocities, good agreement was found between dimensionless values. Maintaining a constant volumetric fill ratio and fabric to drum length ratio for dryers with similar rotational speeds showed comparable time averaged profiles. As such, investigations in to fabric behavior at one scale give a good representation across the range of commercially available appliances. Fabric moisture content was shown to have a marginal impact on fabric and dryer sheet motion, with the velocity for both decreasing during lifting and increasing during free fall. Fabric load size had little effect on lifting behavior but low load sizes were seen to fall much faster and experience high deceleration upon impact. As the volumetric fill fraction in the drum increased, less time was spent by the tracer particle in the bed with a significant increase in time spent in the stagnant core. Work is ongoing to relate the behavior of fabrics and SFE delivery articles to the flow behavior identified here.

#### Nomenclature

$A_{drum}$	Drum wall acceleration ( $m\ s^{-2}$ )
$A_{total}$	Total Eulerian acceleration in a cell ( $m\ s^{-2}$ )
$U_{drum}$	Drum wall velocity ( $m\ s^{-1}$ )



$U_{total}$	Total Eulerian velocity in a cell ( $m\ s^{-2}$ )
$t_{cell}$	Total time spent in a cell (s)
$t_{total}$	Total experimental time (s)
$\Delta$	Difference between two experimental conditions
Fr	Froude number
R	Drum radius (m)
g	Gravitational acceleration ( $m\ s^{-2}$ )
$v_{tracer}$	Linear tracer particle velocity ( $m\ s^{-1}$ )
x	Horizontal tracer coordinate (m)
y	Vertical tracer coordinate (m)
z	Axial tracer coordinate (m)
$\omega$	Drum wall angular velocity ( $rad\ s^{-1}$ )

## Acknowledgments

The authors would like to thank the Positron Imaging Centre team for their support with the PEPT experiments, with special thanks to Dr. Kit Windows-Yule.

## Funding

This work was undertaken as part of an EngD project at the Centre for Doctoral Training in Formulation Engineering, with funding from EPSRC iCASE award EP/R511845/1 (Project reference: 1966258) and Procter and Gamble.

## ORCID

C. R. Jones  <http://orcid.org/0000-0002-3397-4392>  
P. J. Fryer  <http://orcid.org/0000-0003-4767-7839>

## References

- [1] Deans, J. The Modelling of a Domestic Tumbler Dryer. *Appl. Therm. Eng.* **2001**, *21* (9), 977–990. DOI: [10.1016/S1359-4311\(00\)00092-2](https://doi.org/10.1016/S1359-4311(00)00092-2).
- [2] Huelsz, G.; Urbiola-Soto, L.; López-Alquicira, F.; Rechtman, R.; Hernández-Cruz, G. Total Energy Balance Method for Venting Electric Clothes Dryers. *Dry. Technol.* **2013**, *31* (5), 576–586. DOI: [10.1080/07373937.2012.746977](https://doi.org/10.1080/07373937.2012.746977).
- [3] Yadav, V.; Moon, C. G. Modelling and Experimentation for the Fabric-Drying Process in Domestic Dryers. *Appl. Energy*, **2008**, *85* (2–3), 404–419. DOI: [10.1016/j.apenergy.2007.06.014](https://doi.org/10.1016/j.apenergy.2007.06.014).
- [4] Bansal, P. K.; Braun, J. E.; Groll, E. A. Improving the Energy Efficiency of Conventional Tumbler Clothes Drying Systems. *Int. J. Energy Res.*, **2001**, *25* (15), 1315–1332. DOI: [10.1002/er.752](https://doi.org/10.1002/er.752).
- [5] Bansal, P.; Vineyard, E.; Abdelaziz, O. Advances in Household Appliances – A Review. *Appl. Therm. Eng.*, **2011**, *31* (17–18), 3748–3760. DOI: [10.1016/j.applthermaleng.2011.07.023](https://doi.org/10.1016/j.applthermaleng.2011.07.023).
- [6] Ingram, A.; Seville, J. P. K.; Parker, D. J.; Fan, X.; Forster, R. G. Axial and Radial Dispersion in Rolling Mode Rotating Drums. *Powder Technol.* **2005**, *158* (1–3), 76–91. DOI: [10.1016/j.powtec.2005.04.030](https://doi.org/10.1016/j.powtec.2005.04.030).
- [7] Henein, H.; Brimacombe, J. K.; Watkinson, A. P. Experimental Study of Transverse Bed Motion in Rotary Kilns. *Metall. Trans. B* **1983**, *14* (2), 191–205. DOI: [10.1007/BF02661016](https://doi.org/10.1007/BF02661016).
- [8] Mellmann, J. The Transverse Motion of Solids in Rotating Cylinders-Forms of Motion and Transition Behavior. *Powder Technol.* **2001**, *118* (3), 251–270. DOI: [10.1016/S0032-5910\(00\)00402-2](https://doi.org/10.1016/S0032-5910(00)00402-2).
- [9] Govender, I. Granular Flows in Rotating Drums: A Rheological Perspective. *Miner. Eng.* **2016**, *92*, 168–175. DOI: [10.1016/j.mineng.2016.03.021](https://doi.org/10.1016/j.mineng.2016.03.021).
- [10] Silvério, B. C.; Façanha, J. M. F.; Arruda, E. B.; Murata, V. V.; Barrozo, M. A. S. Fluid Dynamics in Concurrent Rotary Dryers and Comparison of Their Performance with a Modified Dryer. *Chem. Eng. Technol.* **2011**, *34* (1), 81–86. DOI: [10.1002/ceat.201000338](https://doi.org/10.1002/ceat.201000338).
- [11] Novak, L.; Širok, B.; Hočevár, M.; Gatarić, P. Influence of Load Mass and Drum Speed on Fabric Motion and Performance of a Heat Pump Tumble Dryer. *Dry. Technol.* **2020**. DOI: [10.1080/07373937.2020.1734608](https://doi.org/10.1080/07373937.2020.1734608).
- [12] Ding, Y. L.; Forster, R. N.; Seville, J. P. K.; Parker, D. J. Scaling Relationships for Rotating Drums. *Chem. Eng. Sci.* **2001**, *56* (12), 3737–3750. DOI: [10.1016/S0009-2509\(01\)00092-6](https://doi.org/10.1016/S0009-2509(01)00092-6).
- [13] Sherritt, R. G.; Chaouki, J.; Mehrotra, A. K.; Behie, L. A. Axial Dispersion in the Three-Dimensional Mixing of Particles in a Rotating Drum Reactor. *Chem. Eng. Sci.* **2003**, *58* (2), 401–415. DOI: [10.1016/S0009-2509\(02\)00551-1](https://doi.org/10.1016/S0009-2509(02)00551-1).
- [14] Yun, C.; Park, S.; Park, C. H. The Effect of Fabric Movement on Washing Performance in a Front-Loading Washer. *Text. Res. J.* **2013**, *83* (17), 1786–1795. DOI: [10.1177/0040517512452927](https://doi.org/10.1177/0040517512452927).
- [15] Wei, Y.; Su, Z.; Zhang, Y.; Li, P.; Yuan, H. The Effect of Fabric Movement on Drying Performance of the Domestic Drum Dryer. *J. Text. Inst.* **2019**, *110* (7), 1059–1071. DOI: [10.1080/00405000.2018.1537104](https://doi.org/10.1080/00405000.2018.1537104).
- [16] Yu, X.; Ding, X. The Transverse Motion of Fabrics in Domestic Tumble Dryers under Different Drying Conditions. *Dry Technol.* **2019**. DOI: [10.1080/07373937.2019.1693398](https://doi.org/10.1080/07373937.2019.1693398).
- [17] Yu, X.; Cao, W.; Ding, X. The Effects of Fabric's Mechanical Properties on Its Motion and Drying Performance in a Domestic Tumble Dryer. *Dry Technol.* **2020**. DOI: [10.1080/07373937.2020.1711523](https://doi.org/10.1080/07373937.2020.1711523).
- [18] Parker, D. J.; Forster, R. N.; Fowles, P.; Takhar, P. S. Positron Emission Particle Tracking Using the New Birmingham Positron Camera. *Nucl. Instrum. Methods Phys. Res. Sect. A* **2002**, *477*, 540–545. DOI: [10.1016/S0168-9002\(01\)01919-2](https://doi.org/10.1016/S0168-9002(01)01919-2).
- [19] Parker, D. J.; Broadbent, C. J.; Fowles, P.; Hawkesworth, M. R.; McNeil, P. Positron Emission Particle Tracking – A Technique for Studying Flow within Engineering Equipment. *Nucl. Inst. Methods Phys. Res. A*, **1993**, *326* (3), 592–607. DOI: [10.1016/0168-9002\(93\)90864-E](https://doi.org/10.1016/0168-9002(93)90864-E).
- [20] Parker, D. J.; Dijkstra, A. E.; Martin, T. W.; Seville, J. P. K. Positron Emission Particle Tracking Studies of Spherical Particle Motion in Rotating Drums.

- Chem. Eng. Sci.* **1997**, 52 (13), 2011–2022. DOI: [10.1016/S0009-2509\(97\)00030-4](https://doi.org/10.1016/S0009-2509(97)00030-4).
- [21] Windows-Yule, C. R. K.; Seville, J. P. K.; Ingram, A.; Parker, D. J. Positron Emission Particle Tracking of Granular Flows. *Ann. Rev. Chem. Biomol. Eng.* **2020**. DOI: [10.1146/annurev-chembioeng](https://doi.org/10.1146/annurev-chembioeng).
- [22] Mac Namara, C.; Gabriele, A.; Amador, C.; Bakalis, S. Dynamics of Textile Motion in a Front-Loading Domestic Washing Machine. *Chem. Eng. Sci.* **2012**, 75, 14–27. DOI: [10.1016/j.ces.2012.03.009](https://doi.org/10.1016/j.ces.2012.03.009).
- [23] Nicuşan, A. L.; Windows-Yule, C. R. K. Positron Emission Particle Tracking Using Machine Learning. *Rev. Sci. Instrum.* **2020**, 91 (1), 13329. DOI: [10.1063/1.5129251](https://doi.org/10.1063/1.5129251).
- [24] Campello, R. J. G. B.; Moulavi, D.; Sander, J. *Density-Based Clustering Based on Hierarchical Density Estimates*. In *Lecture Notes in Computer Science (Including Subseries Lecture Notes in Artificial Intelligence and Lecture Notes in Bioinformatics)*; **2013**; Vol. 7819, LNAI, pp. 160–172. DOI: [10.1007/978-3-642-37456-2\\_14](https://doi.org/10.1007/978-3-642-37456-2_14).
- [25] Bowman, A. W.; Azzalini, A. *Applied Smoothing Techniques for Data Analysis*; Oxford University Press Inc.: New York, **1997**.
- [26] Juarez, G.; Chen, P.; Lueptow, R. M. Transition to Centrifuging Granular Flow in Rotating Tumblers: A Modified Froude Number. *New J. Phys.*, **2011**, 13, 053055. DOI: [10.1088/1367-2630/13/5/053055](https://doi.org/10.1088/1367-2630/13/5/053055).